**Proceedings of the ASME 2023
Pressure Vessels & Piping Conference
PVP2023
July 16-21, 2023, Atlanta, Georgia, USA**

PVP2023-106341

DEVELOPMENT OF A NEW EPRI ELASTIC-PLASTIC FRACTURE MECHANICS HANDBOOK

Ted L. Anderson[1], Robert H. Dodds Jr.[2], Greg V. Thorwald[3], Thomas Dessein[4], Do Jun Shim[5]

[1]TL Anderson Consulting, Cape Coral, FL
[2]Consultant, Longmont, CO
[3]Quest Integrity, Boulder, CO
[4]Integral Engineering, Edmonton, AB, Canada
[5]Electric Power Research Institute, Palo Alto, CA

ABSTRACT

Research funded by the Electric Power Research Institute (EPRI) in the 1980s produced a series of Ductile Fracture Handbooks including J-integral solutions for structural components with cracks. The EPRI Handbook series was to serve as an elastic-plastic equivalent to stress-intensity factor handbooks that various authors published in the 1970s. The original EPRI research in this area significantly advanced the field of elastic-plastic fracture mechanics (EPFM), particularly for ductile instability analysis of structures. However, the initial EPRI Handbooks were restricted to simple two-dimensional configurations, so were of limited practical value. Subsequent EPRI Handbooks published in the late 1980s contained numerous errors, and the technical basis of some solutions was not documented.

Advances in computing technology in the past four decades have now made EPRI's original vision practical. A project is currently underway to produce a new EPRI EPFM Handbook. This project entails over 23,500 3D elastic-plastic finite element analyses of cracked configurations. The process of generating the meshes, editing the input files, running the FEA solver, post-processing the results files, and fitting results to parametric equations is highly automated. Most computations are performed on an EPRI (Linux) cluster with 36, high-end nodes. New parametric equations for the J-integral, crack opening area (through-wall cracks), crack mouth opening displacement, and load-line displacement (laboratory specimen configurations) are developed in this study.

Keywords: Elastic-Plastic Fracture Mechanics, Finite Element Analysis, *J*-Integral

NOMENCLATURE

a	Crack depth
α	Ramberg-Osgood fitting parameter
b	Characteristic length scale in original EPRI J eqn.
β_1	Contained yielding parameter for J-integral
β_3	Contained yielding parameter crack mouth opening displacement (CMOD)
c	Half crack length
E	Young's modulus
ε	Strain
ε_o	Ramberg-Osgood reference strain
ε_{ref}	Reference strain
γ_1	Contained yielding parameter for J
γ_3	Contained yielding parameter for CMOD
h_1	Geometry factor in the original EPRI J eqn.
H_1	Fully plastic fitting parameter for J-integral solutions
H_3	Fully plastic fitting parameter for J-integral solutions
J	J-integral
J_{el}	Elastic component of J
J_{pl}	Plastic component of J
J_{pl}^{CY}	Plastic J under contained yielding conditions
J_{pl}^{FY}	Plastic J under fully yielding conditions
K_I	Mode I stress intensity factor
K_J	Equivalent stress intensity factor computed from J
K_r	Toughness ratio (y-axis) on the FAD

L_r	Load ratio (*x*-axis) on the FAD
m_1	Contained yielding exponent for *J*
m_3	Contained yielding exponent for CMOD
ν	Poisson's ratio
n	Ramberg-Osgood strain hardening exponent
P	Applied load
P_o	Reference load in original EPRI *J* eqn.
R_i	Inside radius of cylindrical shell or elbow
σ	Applied stress
σ_o	Ramberg-Osgood reference stress
σ_{ref}	Reference stress in new EPRI *J* eqn.
σ_{YS}	0.2% offset yield strength
t	Wall thickness
V	Crack mouth opening displacement (CMOD)
V_{el}	Elastic CMOD
Ω_i	Constants on the J versus load relationship; $i = 1, 2, 3$

1. BACKGROUND

Fracture mechanics became an engineering discipline through research performed after World War II. The theoretical underpinnings of linear elastic fracture mechanics (LEFM) emerged in the 1950s and 60s. In 1972, Begley and Landes [1] demonstrated that the *J*-integral [2] could be used to quantify fracture toughness in ductile materials that fail beyond the limits of LEFM.

Fracture stability analyses entail a comparison of crack driving force with fracture toughness. While the work of Begley and Landes addressed fracture toughness measurements for ductile materials using simple test specimens, a rigorous means to infer crack driving force for structural applications beyond the limits of LEFM was lacking in the 1970s. To address this gap in elastic-plastic fracture mechanics (EPFM) technology, the Electric Power Research Institute (EPRI) commissioned research with the goal of generating handbooks of *J*-integral solutions for structural components with cracks. The concept of a *J* handbook was borrowed from existing handbooks that contained elastic stress intensity (K_I) solutions.

Kumar, German and Shih [3], who worked for General Electric (GE), authored the first EPRI Handbook in 1981. This publication, EPRI Report NP-1931, greatly advanced the field of EPFM, particularly for ductile instability analysis of structural components with cracks. The authors of Report NP-1931 developed a parametric equation for the *J*-integral driving force and they fit finite element analysis (FEA) results to this equation. The initial handbook included tables of fitting coefficients for the parametric *J*-integral equation. The *J* solutions in NP-1931 were limited to simple 2D configurations, given the inability of available computing technology to perform 3D elastic-plastic FEA simulations on practical structural components with cracks.

A subsequent EPRI project produced a 3-volume set entitled Ductile Fracture Handbook in 1989 [4]. This handbook set included 3D configurations, but the basis of many of these solutions was not disclosed. Independent attempts to benchmark some of the solutions in [4] revealed numerous errors. Given the limitations in computing capabilities as of 1989, the purported *J*-integral solutions for 3D configurations almost certainly did not arise from an elastic-plastic FEA parametric study.

Now, four decades since publication of the original handbook [3], computing and software technology have evolved to the point where EPRI's original vision can be realized. The authors of this paper are creating a new EPFM Handbook. This EPRI-funded project includes a massive 3D elastic-plastic FEA parametric study with over 23,500 analyses of cracked components. Such an endeavor is made practical with EPRI's (Linux) cluster-server and various software tools that automate much of the workflow. The present authors have developed a new parametric equation for *J* that overcomes limitations of the original formulation in [3].

2. FITTING THE J-INTEGRAL TO FEA SOLUTIONS

2.1 Original EPRI Formulation

Kumar, German and Shih [3] developed a *J* estimation scheme in the form of a parametric equation that divided the *J*-integral into elastic and plastic components:

$$J = J_{el} + J_{pl} \tag{1}$$

The elastic component of *J* is related to the Mode I stress intensity factor as follows:

$$J_{el} = \frac{K_I^{\,2}\left(1-\nu^2\right)}{E} \tag{2}$$

where E is Young's modulus and ν is Poisson's ratio. Consequently, the elastic component of *J* for the configuration of interest can be inferred from the corresponding elastic K_I solution.

The plastic component of *J* is a function of the stress-strain properties of the material. The original EPRI procedure parameterized the material flow properties with the Ramberg-Osgood power-law relationship:

$$\frac{\varepsilon}{\varepsilon_o} = \frac{\sigma}{\sigma_o} + \alpha\left(\frac{\sigma}{\sigma_o}\right)^n \tag{3}$$

where σ_o is a characteristic stress (usually set to the yield strength), $\varepsilon_o = \sigma_o / E$, *n* is the strain hardening exponent, and α is a fitting constant.

Dimensional analysis and a small-strain assumption leads to the following expression for the plastic component of *J:*

$$J_{pl} = \alpha\varepsilon_o\sigma_o b h_1 \left(\frac{P}{P_o}\right)^{n+1} \qquad (4)$$

where b is a characteristic length dimension (*e.g.*, the uncracked ligament length), h_1 is a dimensionless geometry factor, P is a characteristic load, and P_o is a reference load. For a given configuration, h_1 is a function of crack dimensions and n. This dimensionless factor is typically inferred from elastic-plastic finite element analysis. EPRI Report NP-1931[3] includes tables of h_1 values for various 2D configurations.

The authors of NP-1931 noticed discrepancies between elastic-plastic finite element analysis results and J values estimated from Equations (1) to (4). These discrepancies were most pronounced at intermediate load levels between linear elastic and fully plastic deformation. In this intermediate zone, a crack tip plastic zone is surrounded by material subject to elastic loading. The NP-1931 authors attempted to address the discrepancy by incorporating an Irwin plastic zone correction into the elastic component of *J*.

2.2 Contained Yielding vs. Fully-Plastic Deformation

Figure 1 illustrates three stages of loading for a cracked body made from an elastic-plastic material. Under purely elastic loading, LEFM applies and the *J* integral is proportional to load squared:

$$J_{el} = \Omega_1 P^2 \qquad (5)$$

The functional form of Equation (4) applies to fully-yielded conditions:

$$J_{pl}^{FY} = \Omega_2 P^{n+1} \qquad (6)$$

Although the authors of NP-1931 recognized the existence of a contained yielding stage, their approximation with an Irwin plastic zone correction proved inadequate. Given a small plastic zone at the tip of the crack, the plastic component of *J* should be proportional to the plastic work dissipated by crack-tip yielding. The total work in the plastic zone should, in turn, be proportional to the cross-sectional area of the plastic zone on the *x*-*y* plane, where *x* is the direction of crack propagation and *y* is normal to the crack plane. Since the plastic zone radius is proportional to K_I^2 in small-scale yielding, then plastic zone area is proportional to K_I^4, which implies the following relationship for the plastic *J* under small-scale yielding conditions:

$$J_{pl}^{CY} = \Omega_3 P^4 \qquad (7)$$

Equation (7) is not rigorously correct when the plastic zone size is a finite fraction of the remaining ligament, such that small-scale yielding conditions do not apply. Nevertheless, the forgoing heuristic derivation demonstrates that the plastic component of *J* exhibits a different dependence on load under contained yielding compared with the fully yielded condition.

A robust parametric equation for the *J*-integral driving force should capture the transition from linear-elastic to contained yielding to fully plastic behavior. In the present work, the authors formulated such an equation by invoking the failure assessment diagram (FAD) concept, as described below.

2.3 Expressing *J*-Integral Solutions as a Dimensionless Failure Assessment Diagram (FAD)

The failure assessment diagram (FAD) is a fracture map that provides a visual representation of stable and unstable zones for a structural component that contains a crack. Several international standards, including API 579/ASME FFS-1 [5] and the British Standards document BS 7910 [6], have adopted the FAD method to assess fracture stability and flaw tolerance of structures. The FAD is merely a dimensionless representation of the crack driving force.

Given a *J*-integral solution for a structural component, the driving force can be expressed as an equivalent stress-intensity factor by generalizing Equation (2) to elastic-plastic behavior:

$$K_J = \sqrt{\frac{JE}{1-\nu^2}} \qquad (8)$$

The schematic on the left side of Figure 2 illustrates the relationship between K_J and applied stress. The trend is linear when $K_J = K_I$, but the driving force trends upward with plastic deformation. The right side of Figure 2 replots the graph on the left with a dimensionless y axis:

$$K_r = \frac{K_I}{K_J} = \sqrt{\frac{J_{el}}{J}} \qquad (9)$$

Because the elastic component of driving force is in the numerator and total driving force is in the denominator, the curve trends downward with increasing stress.

The *x* axis of Figure 3 can be nondimensionalized with the load ratio, L_r:

$$L_r = \frac{\sigma_{ref}}{\sigma_{YS}} \qquad (10)$$

where σ_{ref} is a reference stress, defined as the nominal applied stress multiplied by a dimensionless geometry factor.

The authors of NP-1931 were among the first to express the *J*-integral driving force as a FAD curve. The FAD is a convenient way to represent *J* solutions visually and remains a useful form for fitting FEA results to a parametric equation.

Standards that implement the FAD method, including API 579/ASME FFS-1 [5], and BS 7910 [6], contain several functional forms for the FAD curve. One such equation accounts for the shape of the stress strain curve:

$$K_r = \left(\frac{E\varepsilon_{ref}}{L_r \sigma_{YS}} + \frac{L_r^{\,3} \sigma_{YS}}{2E\varepsilon_{ref}} \right)^{-1/2} \tag{11}$$

where ε_{ref} is the reference strain, which corresponds to the x coordinate on the uniaxial true stress-strain curve at the reference stress. This functional form captures the linear-elastic, contained yielding, and fully yielded zones, as embodied in Equations (5) to (7).

By setting σ_o in Equation (3) equal to the 0.2% offset yield stress, the Ramberg-Osgood stress-strain model becomes:

$$\varepsilon = \frac{\sigma}{E} + 0.002 \left(\frac{\sigma}{\sigma_{YS}} \right)^n \tag{12}$$

Substituting Equation (12) into (11) gives

$$K_r = \left(1 + L_r^{\,n-1} + \frac{0.5 L_r^{\,2}}{1 + L_r^{\,n-1}} \right)^{-1/2} \tag{13}$$

Invoking Equation (9) yields the following expression for the plastic component of J:

$$J_{pl} = J_{el} \left(L_r^{\,n-1} + \frac{0.5 L_r^{\,2}}{1 + L_r^{\,n-1}} \right) \tag{14}$$

Since the elastic component of J is proportional to P^2 (Equation (5)), the first term in the parenthesis is consistent with the fully-yielded relationship of Equation (6). The numerator of the second term in parentheses follows Equation (7) to capture contained yielding. The denominator of the second term in parentheses causes this term to vanish at high L_r values, such that Equation (14) reduces to Equation (6). In other words, Equation (14) captures contained yielding behavior at low and moderate L_r values, and it reduces to the fully plastic relationship at high L_r.

2.4 New Parametric Equation for FEA Output

Equation (13) is a viable candidate for a nondimensional parametric equation for the J-integral, as it transitions smoothly between the three deformation zones in Figure 1. In the present study, however, certain modifications were found necessary to fit elastic-plastic FEA results for an extensive range of configurations, crack dimensions, and hardening behavior.

The following relationship incorporates additional fitting parameters into Equation (13):

$$K_r = \left[1 + L_r^{\,n-1} + \frac{\beta_1 L_r^{\,m_1}}{1 + \left(\gamma_1 L_r \right)^{n-1}} \right]^{-1/2} \tag{15}$$

The dimensionless parameters β_1, m_1 and γ_1 provide more flexibility to fit J-integral results from elastic-plastic FEA. The reference stress in Equation (10) is given by

$$\sigma_{ref} = H_1 \sigma \left(\frac{0.002E}{\sigma_{YS}} \right)^{\frac{1}{n-1}} \tag{16}$$

where H_1 is a dimensionless fitting parameter and σ is a nominal applied stress. Equation (15) can be written in terms of J:

$$J = J_{el} \left[1 + \left(\frac{\sigma_{ref}}{\sigma_{YS}} \right)^{n-1} + \frac{\beta_1 \left(\frac{\sigma_{ref}}{\sigma_{YS}} \right)^{m_1}}{1 + \left(\gamma_1 \frac{\sigma_{ref}}{\sigma_{YS}} \right)^{n-1}} \right] \tag{17}$$

The above equation contains four dimensionless fitting parameters on the plastic component of J: H_1, β_1, m_1 and γ_1. The dimensionless K_I solution, necessary to compute J_{el}, constitutes a fifth geometry factor.

Figures 3 and 4 show two examples of fits to elastic-plastic FEA J results. The case considered here is an infinitely long external axial crack in a cylindrical shell under internal pressure. Figures 3 and 4 are dimensionless FAD plots for crack depth/thickness (a/t) ratios of 0.2 and 0.6, respectively. The J results for the shallow crack exhibit a traditional FAD shape, but the deeper crack has an unusual shape. Equation (15) captures both cases.

In keeping with the tradition of the original EPRI work [3], the new EPFM Handbook will include fits to additional output from the FEA analyses. Moreover, the present authors have adopted the numbering scheme from EPRI Report NP-1931:

1. H_1, β_1, etc.: J-integral solutions.
2. H_2, β_2, etc.: Load-line displacement in laboratory specimens.
3. H_3, β_3, etc.: Crack mouth opening displacement (CMOD).
4. H_4, β_4, etc.: Crack opening area (COA) in through-wall cracks.

The functional form of Equation (17) applies to all 4 quantities. For example, the parametric equation for CMOD is given by

$$V = V_{el}\left[1+\left(\frac{\sigma_{ref(V)}}{\sigma_{YS}}\right)^{n-1} + \frac{\beta_3\left(\frac{\sigma_{ref(V)}}{\sigma_{YS}}\right)^{m_3}}{1+\left(\gamma_3\frac{\sigma_{ref(V)}}{\sigma_{YS}}\right)^{n-1}}\right] \quad (18)$$

where

$$\sigma_{ref(V)} = H_3\sigma\left(\frac{0.002E}{\sigma_{YS}}\right)^{\frac{1}{n-1}} \quad (19)$$

3. SCOPE OF EPRI EPFM HANDBOOK

The ongoing EPRI EPFM Handbook project entails over 23,500 3D elastic-plastic FEA simulations. Cases in-progress are outlined below. Figure 5 defines the notation for surface and through-wall crack dimensions.

- Cylindrical shells
  - $R_i/t = 2$, 5, 10, 20, 50, 100, ∞ (flat plate). R_i is the inside radius of the cylindrical shell.
  - Axial and circumferential cracks.
  - Internal & external semi-elliptical surface cracks.
    - $a/t = 0.1$, 0.2, 0.3, 0.4, 0.5, 0.6, 0.7, 0.8, 0.9.
    - $c/a = 0.5$, 1, 2, 4, 8, 16, 32, ∞
  - Through-wall cracks.
    - $c/t = 0.5$, 1, 2, 4, 8, 16, 32
  - Internal pressure, axial stress, bending moment load cases. Mixed axial/bending load cases.
- Flat plates
  - Semi-elliptical surface cracks.
    - $a/t = 0.01$, 0.1, 0.2, 0.3, 0.4, 0.5, 0.6, 0.7, 0.8, 0.9.
    - $c/a = 0.5$, 1, 2, 4, 8, 16, 32, ∞
  - Through-wall cracks.
    - $c/t = 0.5$, 1, 2, 4, 8, 16, 32
  - Membrane, bending, and mixed membrane/bending load cases.
- Piping elbows
  - $R_i/t = 4$, 90-degree long radius elbow.
  - Intrados/extrados, axial/circumferential cracks.
  - Internal and external surface cracks.
    - Same dimensions as cylindrical shells.
  - Through-wall cracks.
    - Same dimensions as cylindrical shells.
  - Internal pressure and bending load.
- Piping to elbow girth welds
  - $R_i/t = 4$, 90-degree long radius elbow.
  - Intrados/extrados circumferential cracks.
  - Crack dimensions and load cases same as elbow.
- Laboratory specimens
  - C(T), SE(B), SE(T), M(T) configurations.
- Strain hardening exponent (all configurations)
  - $n = 3$, 5, 7, 10, 15.

Finite element results, including *J*-integral, load-line displacement, crack mouth opening displacement and crack opening area (where appropriate) are fit to the equations described in Section 2.4, and the results tabulated for inclusion in the EPRI EPFM Handbook. The early chapters will contain background information on the technical basis and proper use of the method.

A prototype software application that implements the new method is being developed on the Excel-VBA platform.

4. FEA PARAMETRIC STUDY

The project includes a very large FEA study consisting of over 23,500 3D elastic-plastic analyses that requires significant computing resources. The bulk of analyses are executed on EPRI's Linux cluster (Apollo). The project also requires a high degree of automation through pre-existing software (FEACrack and WARP3D) as well as custom Bash and Python scripts. Two of the authors, GVT and RHD, are the lead developers of FEACrack and WARP3D, respectively, which enabled the project team to modify these products as needed for the present effort.

4.1 FEACrack Software

The FEACrack [7] software automates the generation and post-processing of the many thousand crack meshes needed for this project. A crack mesh is created by entering the geometry, crack location, crack orientation, crack shape, geometry and crack dimensions, and boundary conditions including a load, such as internal pressure. The generated crack mesh is written to a WARP3D FEA input file for analysis. The WARP3D packets results file is post-processed by FEACrack to examine the mesh's deformed shape, stresses, and crack front *J*-integral results. The crack results are extracted to a summary text file for additional curve-fitting of the results. A command line version of FEACrack was created for this project to support scripting automation of the crack mesh generation and post-processing so that batches of models can be created, run, and post-processed using the Linux cluster computer.

Figures 6 to 9 show typical meshes for cracks in a cylindrical shell. All models use 20-node isoparametric elements with reduced integration. The crack face color is light blue. The red, green, and orange mesh colors show the mesh zones used to adjust mesh refinement near the crack plane.

4.2 WARP3D Finite Element Code

WARP3D [8] is an open-source nonlinear finite element code optimized for fracture mechanics modeling. This software has been developed over multiple decades by one of the authors (RHD), along with his graduate students and postdoctoral fellows at the University of Illinois Department of Civil Engineering.

Two compelling reasons led to use of WARP3D for this project rather than a commercial FEA program such as Abaqus or ANSYS:

1. No licensing costs are associated with WARP3D – tens of instances of the code may be executed concurrently across the cluster with each instance also running in parallel.
2. The open-source feature enabled certain modifications described below.

Nonlinear analyses of models with cracks and computations of *J* values require care in the selection of suitable load step sizes to ensure convergence of the global iterations and tracking of path-dependent plastic deformation (the solutions employed J_2 flow-theory plasticity and a small-geometry change formulation). The appropriate step size typically varies throughout the analysis as plasticity evolves along the crack front. Moreover, a sufficient set of results is needed for each simulation to fit Equation (15) in the elastic, contained yielding, and fully plastic regions. Because the present study considers a wide range of geometries, crack dimensions and hardening levels, there exists no single set of load steps suitable for all models. Consequently, an *adaptive, J-based load stepping algorithm* has been incorporated into WARP3D (included in the open-source code) that removes the need to specify load step sizes.

The adaptive load stepping algorithm chooses the next step size in the sequence based on two criteria: the rate of increase of the J/J_{el} ratio at the maximum *J* location on the front, or the decrease in K_r, where $K_r = 1/\sqrt{J/J_{el}}$. The analysis ends when a specified J/J_{el} is reached.

The K_r value proves the most effective metric early in the loading. Initially, $K_r = 1.0$ and gradually decreases with the buildup of plasticity along the crack front. The adaptive code increases or decreases the step sizes to maintain a user-specified decrease in K_r per step (*e.g.* $\Delta K_r = 0.05$).

Once K_r decreases to a value indicating moderate plastic deformation (*e.g.*, 0.6-0.8), the adaptive algorithm switches to the J/J_{el} ratio to define the sizes of subsequent load steps that generate values for the larger L_r values. The user specifies a target value for the change in J/J_{el} over each load step, often 0.1-0.3. This ratio is computed once the Newton iterations for the load step converge, and the domain integral computations are completed. After a few load steps, the adaptive algorithm is quite effective at adjusting load step sizes to maintain the target increment in J/J_{el}. A typical solution uses 100-150 load steps to define the full extent of the FAD curve for a given configuration.

4.3 FEA Workflow

Figure 10 shows the workflow in the FEA parametric study. An FEACrack input file (*.ELT) contains data for geometry, component dimensions, crack location/orientation, crack dimensions, material properties, and boundary conditions. A single ELT file generally contains dimensions for multiple cracks. Example: for semi-elliptical surface cracks in cylindrical shells, plates and elbows, the ELT file for a given set of component dimensions and boundary conditions contains data for 63 crack sizes, which generates 63 WARP3D input files (*.inp). The command line version of the FEACrack mesh generator mentioned in Section 4.1 performs batch processing of multiple ELT files in a directory; a single command produces a large number of .inp files.

Normally, a .inp file created with FEACrack is ready to run in the solver. In this project, the stress-strain data are omitted from the .inp files created by the mesh generator. Moreover, only the first load step with a quite small size (linear-elastic) is specified in the .inp file; subsequent steps are determined in the adaptive algorithm. Bash/Python scripts create 5 copies of each .inp file to include the stress-strain data corresponding to n = 3, 5, 7, 10, and 15 and also include adaptive load stepping commands in each input file.

Mesh generation and .inp file editing are performed locally on Windows/Mac workstations. The completed .inp files in groups often exceeding 500 are then moved to the EPRI Apollo cluster, where Bash/Python scripts manage submission of the analyses and organization of the many thousands of result files. In a typical set, WARP3D executes concurrently on 25-30 cluster nodes with each instance using 25 threads (cores) on each node. When WARP3D completes each analysis, scripts execute the command-line version of the FEACrack post-processor which writes the *J*-integral results into a more compact text file, as well as the displacements of selected node sets. The latter are used to infer load line displacement, crack mouth opening displacement, and crack opening area (as appropriate). The compact, crack results files are also used in curve fitting as described below.

4.4 Fitting Procedures

Given the large number of FEA cases produced within the project, the process to find the 4 plastic fitting coefficients, in Equations (15) to (19) has been fully automated. The procedure seeks to fit coefficients that vary smoothly with the geometry variables and the hardening exponent, as shown in Figure 11 for H_1. The end-user can then interpolate the coefficients directly rather than needing to interpolate the computed *J* integral curves. This was achieved using the following procedure:

1. The curve-fitting optimization is performed on a case that is central across the space of geometry variables and hardening exponent, Figure 11 (a). In the first pass, only the H_1, β_1 and m_1 parameters are fit and the γ_1 parameter is held fixed with a value of 1.0.
2. The H_1, β_1 and m_1 results of the central case set the starting seeds for the curve-fitting optimization of the adjacent cases in the space of geometry variables and hardening exponent.
3. The curve fitting continues, moving outwards from the central cases, using the results of the nearest adjacent case as the starting seed for the optimization.

4. Once all cases are fit, using the previous solutions, allow the optimization to re-compute all 4 of the plastic fitting coefficients.
5. Develop a radial basis function (RBF) to the results of each fitting coefficient across the space of the geometry variables and hardening exponent [9]. Use the RBF to identify cases where the optimization has converged to a local optimum that is off trend from the adjacent cases. Re-fit the RBF with the off-trend cases excluded and use this RBF to select new seeds to re-fit the case. Repeat Step 5 until no cases are left that are assessed as off trend.

5. CONCLUDING REMARKS

EPRI's original vision of an EPFM Handbook was impractical in the 1980s but is coming to fruition with the aid of modern computer hardware and software. The computational effort undertaken in this project is unprecedented in the field of nonlinear fracture mechanics. The new Handbook will include tables of fitting coefficients for over 23,000 FEA solutions. Future efforts can focus on expanding the library of elastic-plastic crack solutions. In addition, a prototype software application that implements the new method is being developed on the Excel-VBA platform.

ACKNOWLEDGEMENTS

This work was funded by the Electric Power Research Institute (EPRI) Materials Reliability Program (EPRI Task ID: 1-115151-01-01). Jaydon Vanselow of Integral Engineering contributed to the development of the fitting procedures.

REFERENCES

[1] Begley, J. A. and Landes, J.D., "The J-Integral as a Fracture Criterion." ASTM STP 514, American Society for Testing and Materials, Philadelphia, 1972, pp. 1-20.

[2] Rice, J.R. "A Path Independent Integral and the Approximate Analysis of Strain Concentration by Notches and Cracks." *Journal of Applied Mechanics*, Vol. 35, 1968, pp. 379-386.

[3] Kumar, V., German, M.D., and Shih, C.F., "An Engineering Approach for Elastic-Plastic Fracture Analysis." EPRI Report NP-1931, Electric Power Research Institute, Palo Alto, CA, 1981.

[4] Zahoor, A. "Ductile Fracture Handbook" Three-Volume Set, EPRI Report NP-6301, Electric Power Research Institute, Palo Alto, CA, 1989.

[5] API 579-1/ASME FFS-1, *Fitness-for-Service*, jointly published by the American Petroleum Institute and the American Society for Mechanical Engineers, 2021.

[6] BS 7910:2019, "Guidance on Methods for Assessing the Acceptability of Flaws in Metallic Structures." British Standards Institution, London, 2019.

[7] Quest Integrity USA, LLC, FEACrack version 3.2.37 (2022), Boulder, CO, www.questintegrity.com/software-products/feacrack.

[8] WARP3D. www.warp3d.net.

[9] Buhmann, M.D., *Radial Basis Functions: Theory and Implementations.* Cambridge University Press, 2003.

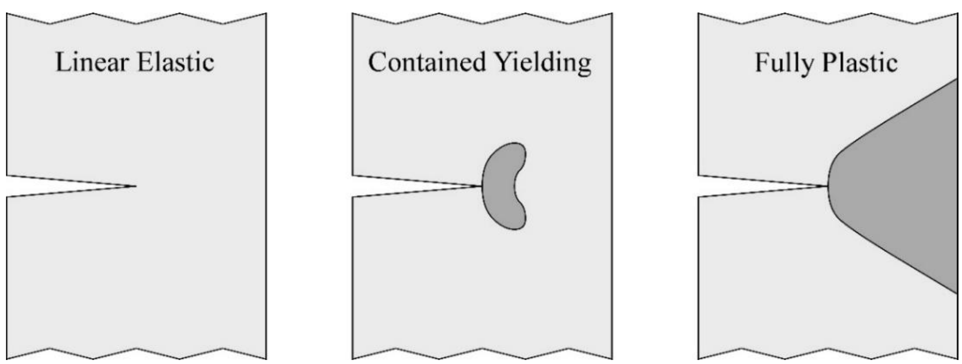

FIGURE 1: THREE ZONES OF DEFORMATION IN A CRACKED BODY.

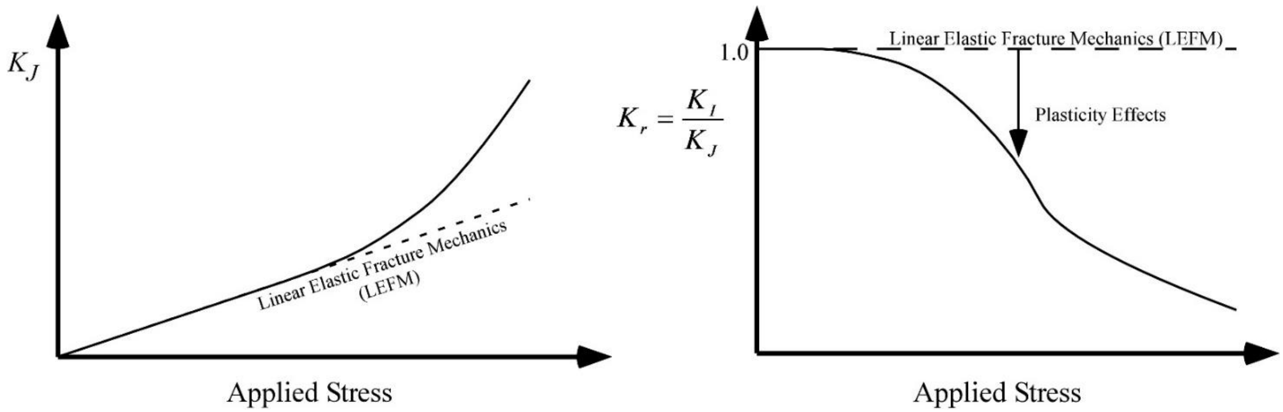

FIGURE 2: CRACK DRIVING FORCE, K_J, AS A DIMENSIONLESS RATIO TO CREATE A FAD CURVE.

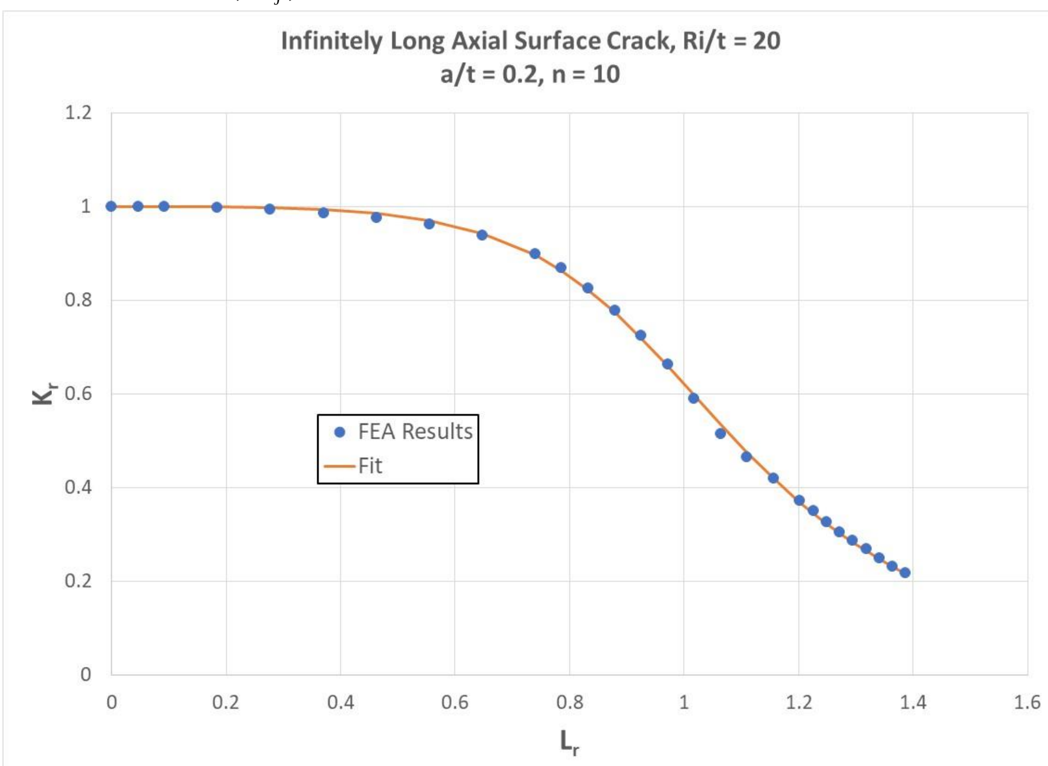

FIGURE 3: FIT OF *J* RESULTS FOR A LONG EXTERNAL AXIAL SURFACE CRACK WITH $a/t = 0.2$.

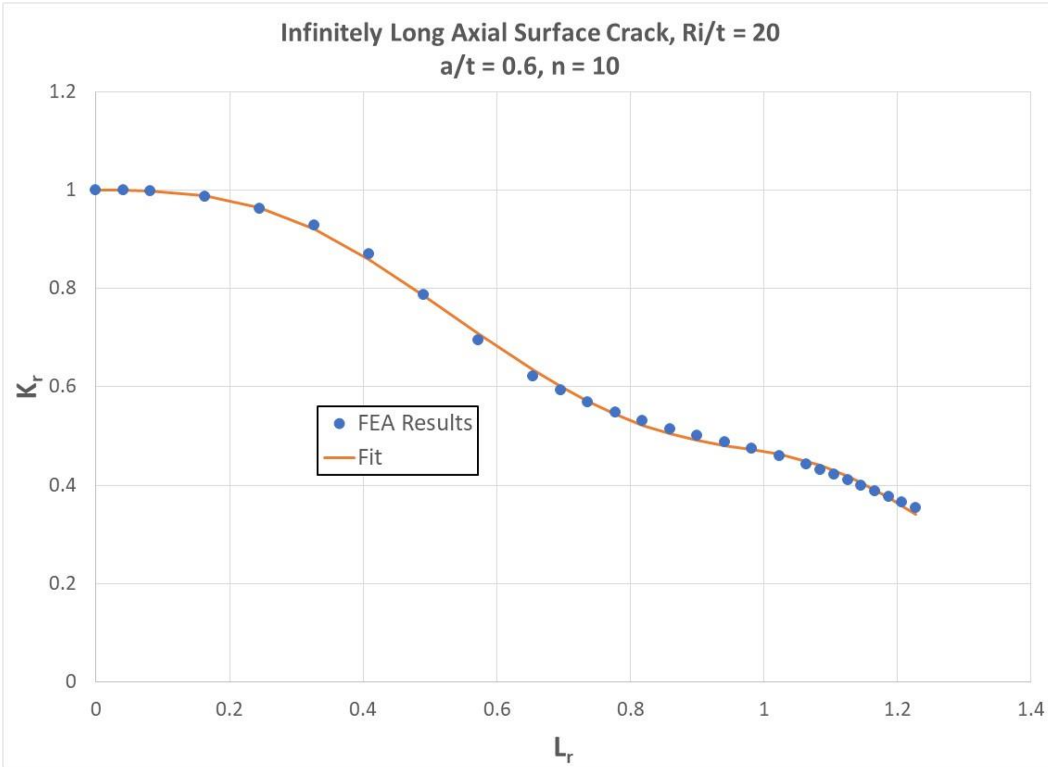

FIGURE 4: FIT OF *J* RESULTS FOR A LONG EXTERNAL AXIAL SURFACE CRACK WITH $a/t = 0.6$.

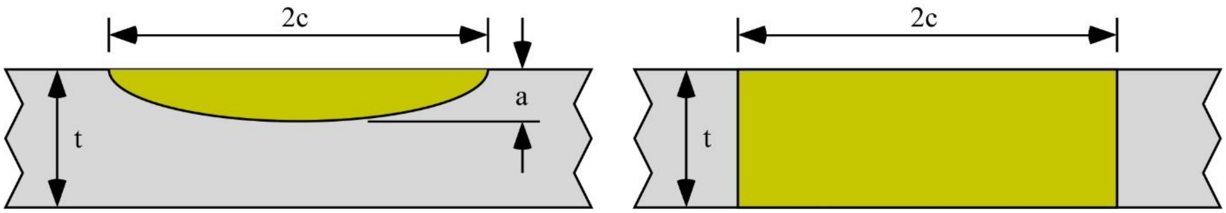

FIGURE 5: CRACK DIMENSIONS FOR SURFACE AND THROUGH-WALL CRACKS.

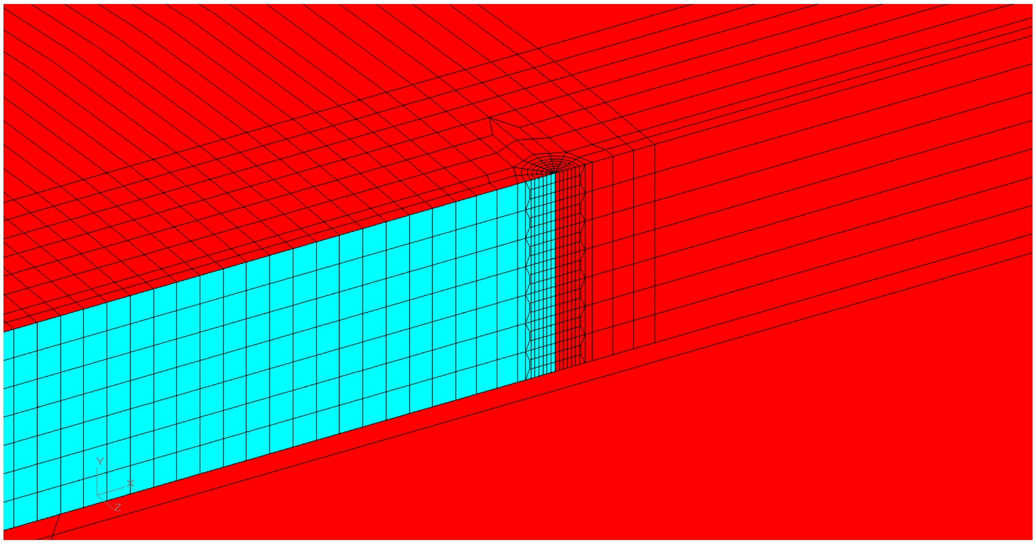

FIGURE 6: FINITE ELEMENT MESH FOR AN AXIAL THROUGH-WALL CRACK IN A CYLINDRICAL SHELL.

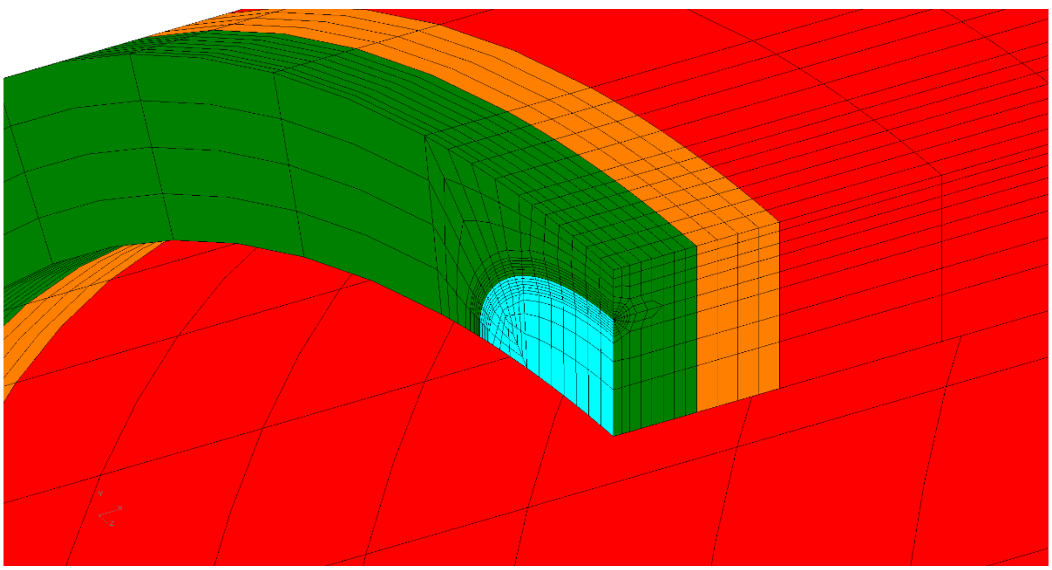

FIGURE 7: FINITE ELEMENT MESH FOR AN INTERNAL CIRCUMFERENTIAL SURFACE CRACK IN A CYLINDRICAL SHELL.

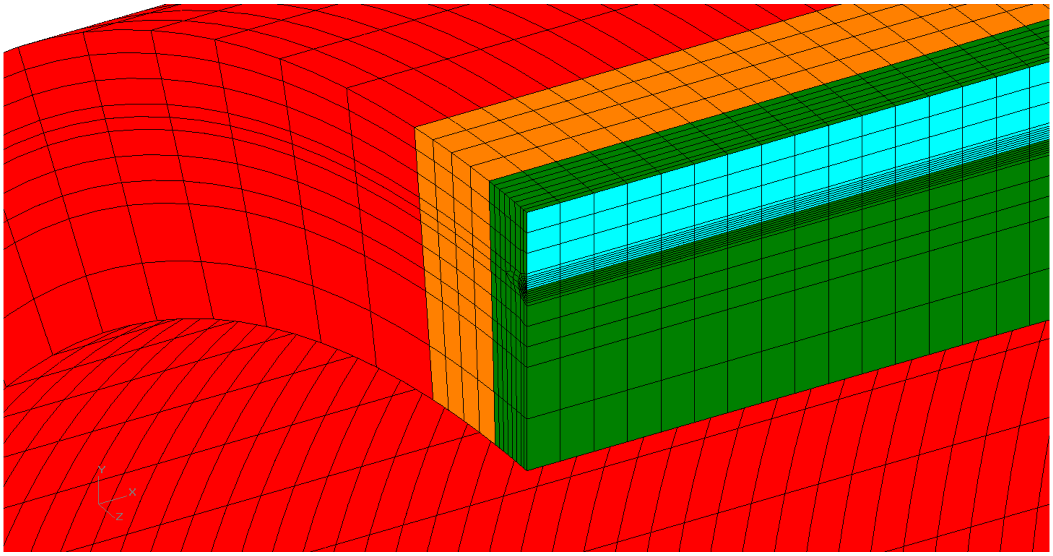

FIGURE 8: FINITE ELEMENT MESH FOR AN EXTERNAL AXIAL SURFACE CRACK WITH INFINITE LENGTH.

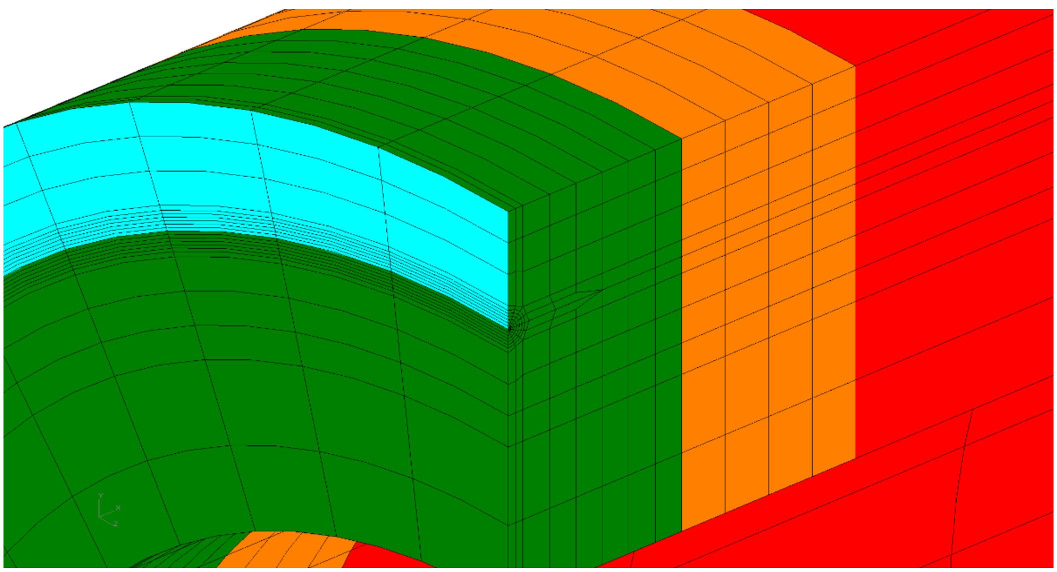

FIGURE 9: FINITE ELEMENT MESH FOR AN EXTERNAL 360-DEGREE CIRCUMFERENTIAL CRACK IN A CYLINDRICAL SHELL.

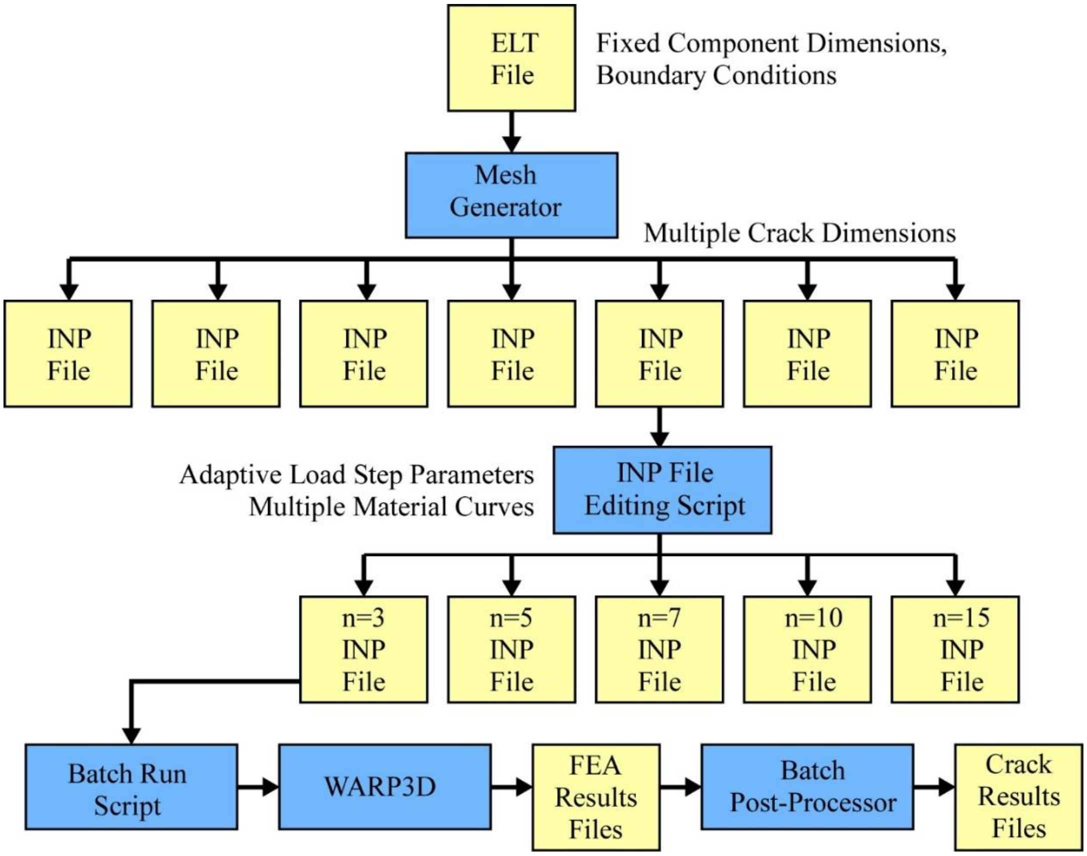

FIGURE 10: WORKFLOW FOR THE FEA PARAMETRIC STUDY.

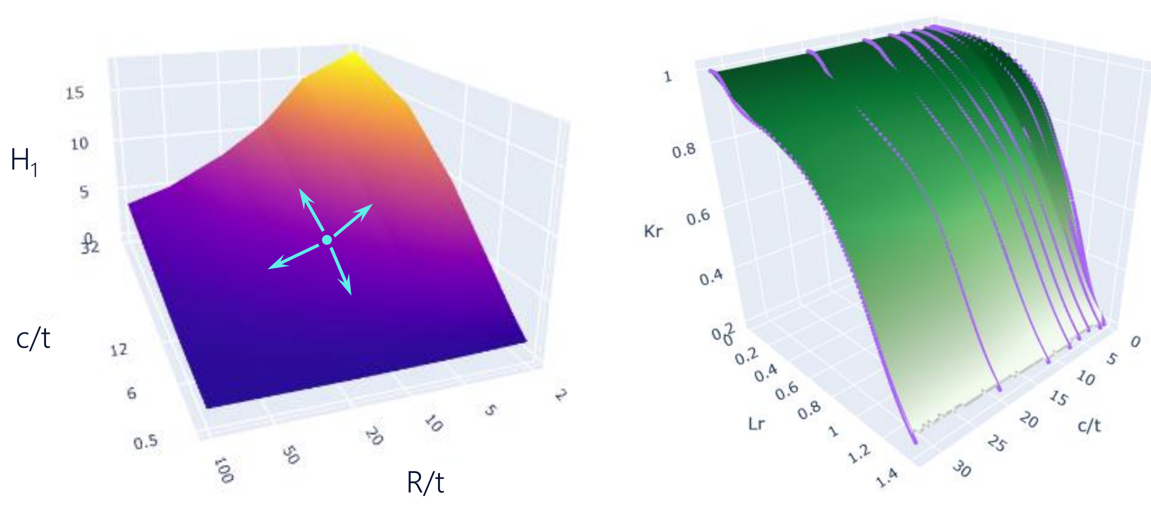

(a) (b)

FIGURE 11: CURVE FITTING RESULTS FOR AXIAL THROUGH-WALL CRACKS WITH VARYING c/t RATIOS SHOWING (a) A SMOOTH TREND IN PLASTIC FITTING COEFFICIENT H_1 AND (b) AN ACCURATE REPRESENTATION OF THE FEA RESULTS AND SMOOTH INTERPOLATED FAD CURVES.